Photoelectron imaging of carbonyl sulfide cluster anions: Isomer coexistence and competition of excited-state decay mechanisms

Eric Surber and Andrei Sanov
Department of Chemistry, University of Arizona, Tucson, Arizona 85721-0041

(Received 22 January 2003; accepted 5 March 2003)

We investigate the structure and decay of $(OCS)_n^-$ cluster ions ($n=2-4$) using photoelectron imaging spectroscopy. The results indicate the coexistence of isomers with OCS^- and covalently bound $(OCS)_2^-$ cluster cores. A several-fold decrease in the relative abundance of the dimer-based species is observed for $n=3$ and 4 compared to $n=2$. The $OCS^-(OCS)_{n-1}$ cluster ions undergo direct photodetachment similar to $OCS^- \cdot H_2O$, while $(OCS)_2^-(OCS)_{n-2}$ exhibits both direct electron detachment and cluster decomposition via ionic fragmentation and autodetachment. The autodetachment originates from either the excited states of the parent cluster or internally excited anionic fragments. It is described using a statistical model of thermionic emission, which assumes rapid thermalization of the excitation energy. A decrease in the relative autodetachment yield in the trimer and tetramer cluster ions, compared to the covalent dimer, is attributed to competition with ionic fragmentation. © *2003 American Institute of Physics.* [DOI: 10.1063/1.1569915]

I. INTRODUCTION

Gas-phase clusters are ideal for studies of chemical interactions and reaction dynamics at the molecular level. Despite their (sub)nanoscale size, they retain some characteristics of the bulk media, in particular the coupled behavior of the constituents. The transition between the gas-phase and bulk properties of matter has been the subject of extensive research[1] centered about one recurring question: how much matter is needed for physical laws associated with bulk materials to be applicable?[2]

We describe photoelectron imaging experiments, in which both the molecular and ''bulk'' properties are manifest in the single-photon excitation of small cluster anions of carbonyl sulfide. The photoelectron images unveil the coexistence of the $OCS^-(OCS)_{n-1}$ and $(OCS)_2^-(OCS)_{n-2}$ isomers and shed light on the electronic structure and excited-state dynamics of the latter species. The results show that the applicability of the bulk description to gas-phase systems is determined by the details of the electronic structure, rather than merely the size of the microscopic object.

The $(OCS)_n^-$ cluster anions exhibit rich and largely unexplored photochemistry.[3] While the isovalent $(CO_2)_n^-$ and $(CS_2)_n^-$ clusters have been the subject of many experimental[4–22] and theoretical[17,20,21,23,24] studies, only one previous experiment investigated the interaction of $(OCS)_n^-$ with light.[3] Since cluster reactivity[25] and dynamics are largely determined by the ionic core, a fundamental question regarding all three of the above cluster families is whether the excess electron is localized on a single monomer or shared between two (or more) monomer moieties.[1,13,14,17–20,23,24] The charge localization or sharing lead to different electronic and structural isomers, which have been observed for $(CO_2)_n^-$ and $(CS_2)_n^-$,[18,19,22] and hypothesized for $(OCS)_n^-$.[3] For example, the $(CO_2)_n^-$ photoelectron spectra reveal discontinuities in the dependence of the vertical detachment energy (VDE) on cluster size.[14,18] These were attributed to cluster core switching between the covalently bound $(CO_2)_2^-$ and CO_2^- monomer anions. The electronic structure calculations of Fleischman and Jordan predicted that the $(CO_2)_2^-$ global minimum corresponds to a D_{2d} symmetry structure with the excess electron shared between the two CO_2 groups.[23] However, due to the more effective solvation of the monomer anion, the CO_2^--based clusters are more stable in the range of $n=7-13$.[14,18]

Isolated OCS^- is believed to be metastable,[26,27] but the addition of solvent molecules—e.g., H_2O or OCS—yields a stable cluster anion.[3,26,28] The monohydrated anion was predicted to have a straightforward electrostatically bound $OCS^- \cdot H_2O$ structure,[26,28] while replacing water with OCS gives way to the electrostatically and covalently bound isomers described as $OCS^- \cdot OCS$ and $(OCS)_2^-$. The two types of the dimer species differ not only in their geometric structures, but also in the electronic configurations, and hence are viewed as both structural and electronic isomers.[3,29] At least two covalent $(OCS)_2^-$ species were predicted theoretically.[3,29] The most stable has an equilibrium structure of C_{2v} symmetry with the C–C and S–S bonds of the orders of 1 and 1/2, respectively, and a number of low-lying excited states. The existence of the covalent dimer anion and its solvated species was indirectly indicated in $(OCS)_n^-$ photofragmentation.[3] The significant yield of S_2^- and S_2^--based fragments was attributed to the breakup of a chromophore, in which two sulfur atoms are bound by covalent interaction.

The photofragmentation and photodetachment studies complement each other, exploring competing reaction pathways. Due to the low thresholds for both detachment and dissociation, the competition between electron emission and fragmentation plays an important role in $(OCS)_n^-$. In some of the fragmentation channels, autodetaching products may be formed, while, on the other hand, the parent autodetachment (AD) itself can be safely assumed to be dissociative.

Thus the excited-state decay ties the ionic fragmentation and AD into an entangled knot of a decomposition reaction, which involves several competing pathways potentially leading to the same final products.

In two recent papers,[30,31] we reported photoelectron imaging studies of the homogeneous and heterogeneous solvation of OCS^- by OCS or H_2O. We discussed two electron-emission mechanisms apparent in $(OCS)_2^-$ at 800, 530, and 400 nm: direct photodetachment and AD.[31] On the other hand, only the direct detachment was observed for $OCS^- \cdot H_2O$.[30] Since the highest-occupied molecular orbital (HOMO) and hence the detachment dynamics of $OCS^- \cdot OCS$ are expected to resemble those of $OCS^- \cdot H_2O$, we used the comparison of the $(OCS)_2^-$ and $OCS^- \cdot H_2O$ results to single out the signatures of $OCS^- \cdot OCS$ and identify the contributions of the covalent dimer.[31]

The AD originating from photoexcited $(OCS)_2^-$ (or its ionic fragments) was described[31] as a cluster analog of thermionic emission (TE), an effect usually associated with bulk materials.[32] It was suggested that the applicability of the bulk description depended on the availability of low-lying yet strongly mixed excited states.[31] The bulk TE model assumes that efficient electron–phonon couplings lead to rapid thermalization of the excitation energy among the electronic and nuclear degrees of freedom.[32,33]

Analogs of TE have been previously seen in the gas phase—for example, in fullerenes.[33,34] The gas-phase manifestations of TE include a thermal electron kinetic energy (eKE) distribution, the delayed and consequently isotropic nature of the electron emission.[33] In contrast, direct photodetachment is fast and in general anisotropic. Concerning negative ions, the Neumark group described TE in the multiphoton detachment of C_4^-, C_6^-, and C_8^-.[35] Baguenard *et al.* observed this effect in the ultraviolet photodetachment of carbon[36] and tungsten[32] cluster anions.

The $(OCS)_n^-$ clusters described here present special interest, because their decay involves acute competition between autodetachment and fragmentation. In this work, we exploit the crucial advantages of imaging[37] to obtain evidence of the existence and dynamics of excited anionic states of $(OCS)_n^-$. Imaging is ideally suited to detection of both slow and fast photoelectrons, which is important for the simultaneous observation of autodetachment and direct photodetachment. The photoelectron angular distributions are also easily visualized, helping elucidate the emission mechanisms.

We expand our initial report[31] on $(OCS)_2^-$ to include $(OCS)_n^-$ clusters up to $n=4$. In addition, the range of photon energies is extended to include 267 nm, where higher-energy transitions, not seen previously, are observed. We explore the variations in the relative abundances of the $OCS^-(OCS)_{n-1}$ and $(OCS)_2^-(OCS)_{n-2}$ isomers under the conditions of stepwise solvation and the competition between AD and ionic fragmentation.

The next section describes the experimental apparatus used in this study. Section III presents the results, followed by the model and analysis details given in Sec. IV. Section V discusses the implications of the results, focusing on the coexistence of the dimer- and monomer-anion-based clusters and the competition of decay mechanisms. A summary of the paper is given in Sec. VI.

II. EXPERIMENTAL APPARATUS

The experiments are carried out using a negative-ion photoelectron imaging apparatus, whose detailed description is given elsewhere.[22,26,38] In brief, it consists of a pulsed ion source, a time-of-flight (TOF) ion mass-spectrometer, and a photoelectron imaging assembly.

The $(OCS)_n^-$ cluster ions are formed as described previously,[3,26] using published cluster–ion techniques.[39] The ions are generated in an electron-impact ionized pulsed supersonic expansion of a 7% mixture of OCS in Ar. They are pulse extracted through a 4-mm-diam orifice into a 1.7-m-

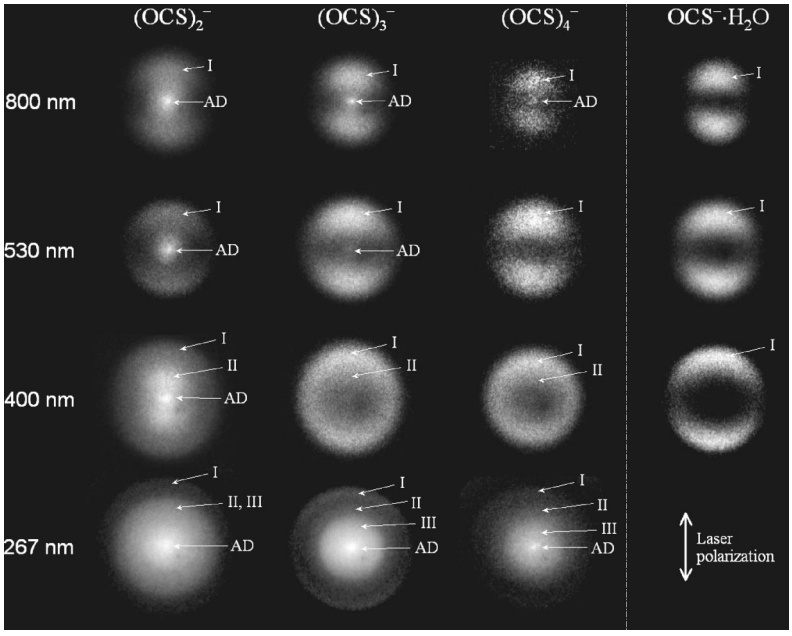

FIG. 1. Photoelectron images of $(OCS)_{2-4}^-$ and $OCS^- \cdot H_2O$ recorded at 800, 530, 400, and 267 nm. The images are shown on arbitrary velocity and intensity scales (see Figs. 2–4 for quantitative information). Arrows indicate the contributions of autodetachment (AD) and direct detachment bands I, II, and III.

long Wiley–McLaren TOF mass spectrometer, where they are accelerated to a kinetic energy of about 2.3 keV. The ion beam is steered and focused using electrostatic deflectors and an Einzel lens, and referenced to ground potential, without affecting the kinetic energy, using a fast potential switch.[40] After passing through two differentially pumped regions, the ions enter the detection chamber with a base pressure of $\sim 3\times 10^{-9}$ torr.

The ions are detected at the end of the flight tube using a dual microchannel plate (MCP) detector with a metal anode (Burle, Inc.). The resulting mass spectrum[26] is used to identify the size-selected clusters and adjust the experiment timing to overlap laser pulses with the desired species. The photoelectrons are detected in the direction perpendicular to the ion beam, using the imaging method of Chandler and Houston[37] in the velocity-mapping implementation of Eppink and Parker.[41] The 40-mm-diam MCP detector with a phosphor screen (Burle, Inc.) is mounted at the end of a 15-cm-long electron flight tube and monitored using a CCD camera (CoolSnap, Roper Scientific). The images are averaged for $1-5\times 10^4$ experimental cycles. To discriminate against noise, the MCPs are operated in a pulsed-bias mode: the total bias across the two plates, normally kept at 1.0–1.2 kV, is pulsed to 1.8 kV for a 300-ns window within which the arrival of the photoelectrons is expected. The velocity-map focusing was optimized and the eKE calibration was determined using the detachment transitions in I^- at 267 nm.[22]

The laser radiation is produced by an amplified Ti:sapphire laser system from Spectra Physics (1 mJ, 100-fs pulses). The 800-nm measurements use a portion ($\sim$200 μJ/pulse) of the unfocused fundamental output. The 530-nm radiation (30–50 μJ/pulse) is generated by sum-frequency mixing the output of the optical parametric amplifier with the fundamental. The 400- and 267-nm light is produced by frequency doubling or tripling a portion of the fundamental in the Super Tripler harmonics generator (Super Optronics), giving 120 or 40 μJ/pulse, respectively. The 530-, 400-, and 267-nm beams were mildly focused with a 2-m focal-length lens, positioned 1.3 m before the interaction region. The polarization axis was always arranged parallel to the imaging detector plane. The single-photon nature of the observed transitions was verified using the signal power dependence.

III. RESULTS

Figure 1 gives an overview of the results for $(OCS)_n^-$, $n=2-4$. For all three cluster sizes, the images were recorded at 800, 530, 400, and 267 nm, with the laser polarization vertical in the plane of all images. The 800-, 530-, and 400-nm images obtained previously in the photodetachment of $OCS^-\cdot H_2O$ are also shown for comparison.[30] Despite the overall differences between the homogeneous and heterogeneous cluster anions, the higher-eKE parts of $(OCS)_n^-$ images resemble those of $OCS^-\cdot H_2O$ at all wavelengths for which the comparison is available. To the contrary, the mid- and low-eKE parts are qualitatively different. In particular, we note the central spots in the $(OCS)_n^-$ images, which are not present in the $OCS^-\cdot H_2O$ results and neither were they seen for $OCS^-(H_2O)_2$.[30]

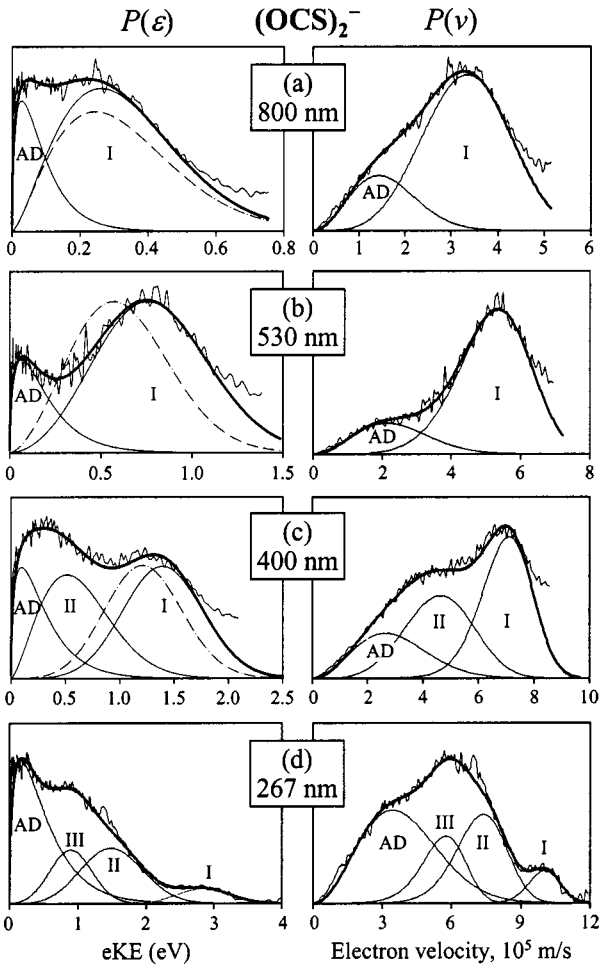

FIG. 2. Experimental and simulated $(OCS)_2^-$ photoelectron spectra in the energy and velocity domains (left and right columns, respectively). The experimental spectra (thin lines with apparent noise) are derived from the corresponding images in Fig. 1. The simulated spectra are shown by bold lines with the individual transitions (AD and bands I, II, and III) indicated by the thin curves, correspondingly labeled. The dashed curves in (a)–(c) [$P(\varepsilon)$ column, this figure only] are fits [Eq. (5)] to the $OCS^-\cdot H_2O$ spectra (not shown).

The images are analyzed using the inverse Abel transformation,[42] from which the velocity and angular distributions were obtained. The Abel inversion and subsequent integration of the transformed images was carried out using the basis set expansion (BASEX) method of Reisler and co-workers.[43] The velocity distributions $P(v)$ are converted into photoelectron energy spectra $P(\varepsilon)$ ($\varepsilon \equiv$ eKE) according to the straightforward relation

$$P(\varepsilon)=P(v)dv/d\varepsilon \propto P(v)/v. \tag{1}$$

The $P(\varepsilon)$ and $P(v)$ distributions obtained for $(OCS)_n^-$, $n=2$, 3, and 4, are shown in Figs. 2, 3, and 4, respectively. Traditionally, photoelectron spectra are analyzed in the energy domain, and thus the velocity spectra in the left columns of Figs. 2–4 may appear redundant. However, imaging experiments provide *velocity* rather than *energy* maps of the detachment process. We find it important to model the results in the velocity domain inherent in imaging, for two reasons: (i) the information seen in velocity spectra is not always clear in the energy spectra, particularly for slow electrons;

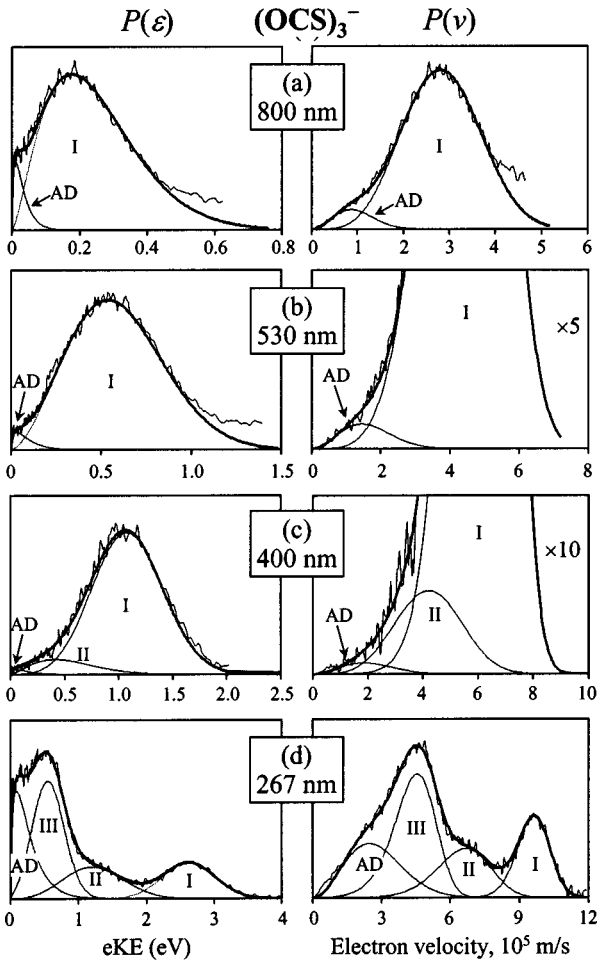

FIG. 3. Experimental and model spectra for $(OCS)_3^-$. See Fig. 2 caption for further details. The $P(v)$ distributions in (b) and (c) are magnified 5× and 10×, respectively, to highlight the autodetachment components.

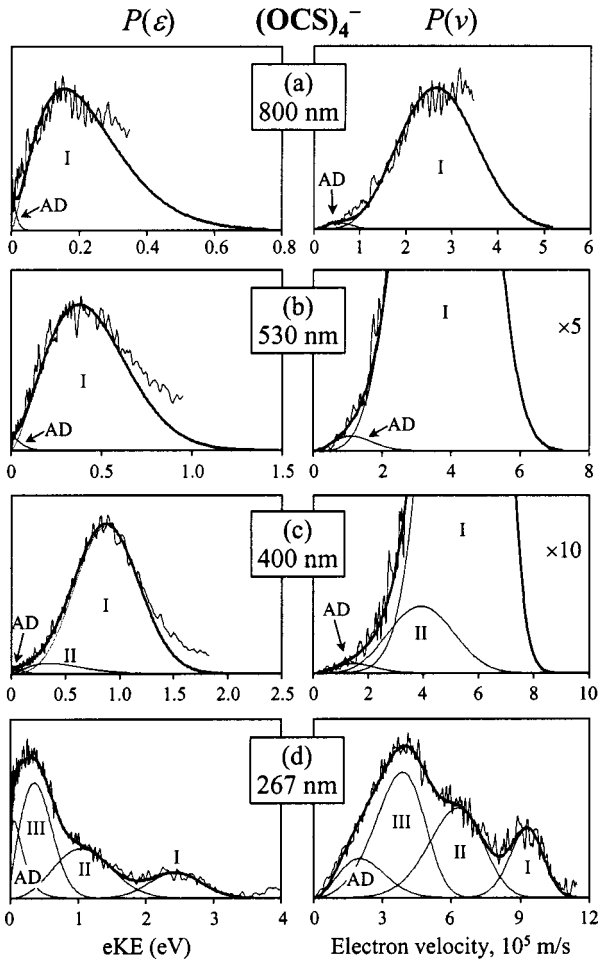

FIG. 4. Experimental and model spectra for $(OCS)_4^-$. See Fig. 2 caption for further details. The $P(v)$ distributions in (b) and (c) are magnified 5× and 10×, respectively, to highlight the autodetachment components.

(ii) the experimental resolution (defined as Δv) is constant in the velocity domain, making the statistical analysis of the data more favorable there than in the energy domain.

Both $P(\varepsilon)$ and $P(v)$ reflect a reduction of information provided by the experiment. Imaging allows discernment of transitions that are unresolved in the spectra. For example, the 400-nm $(OCS)_2^-$ spectra in Fig. 2(c) appear to consist of only two bands, while the corresponding image in Fig. 1 clearly reveals three transitions.

IV. ANALYSIS

Examination of the images reveals the contributions of two electron-emission mechanisms. The isotropic spots at image centers correspond to indirect decay via delayed electron emission (autodetachment), while the anisotropic bands at higher eKEs are associated with direct detachment transitions. The signals at image centers cannot be attributed to direct detachment bands (e.g., low-energy wings of bands with VDE$>h\nu$), because, uncharacteristic of direct photodetachment, the central spots appear in images independent of the wavelength.

We model the results with simulated spectra accounting for both the indirect and direct mechanisms. First, the AD bands are modeled using the delayed thermionic emission formalism,[33] as employed by Baguenard *et al.*[32,36] Our core assumption is that the available energy is distributed statistically among all product degrees of freedom. Despite the competition between AD and ionic fragmentation, the TE model is applicable to the final product distributions (i.e., the photoelectron spectra), provided the statistical assumption is valid at all decay stages. Second, the direct detachment transitions are described using a simplified Franck–Condon model.

Autodetachment. In the TE model applied to negative ions, the eKE distribution of the emitted electrons is approximated by Klots' formula[32,33,44]

$$P_{\mathrm{TE}}(\varepsilon) \propto \varepsilon^{1/2} \exp(-\varepsilon/k_B T_{\mathrm{TE}}). \tag{2}$$

It assumes a completely statistical emission process within the constraints of the detailed balance principle. The pre-Boltzmann factor reflects the cross-section scaling due to the effect of the centrifugal barrier, and T_{TE} describes the effective temperature of the emission spectrum. Under the condition of thermal equilibrium, T_{TE} corresponds to the microcanonical ''daughter'' temperature of the remaining neutral cluster. This temperature should not be confused with Klots' ''isokinetic'' or emission temperature, controlling the decay rate.[33] Following the thermalization of the excitation energy

$(h\nu)$, T_{TE} is determined by the microcanonical temperature of the parent cluster corrected for the energy required for emitting an electron, i.e., the adiabatic electron affinity (EA):[32,36]

$$T_{TE} \approx T_0 + (h\nu - EA)/C_v . \quad (3)$$

Here T_0 is the cluster temperature prior to the photon absorption, which we take as ~70 K,[39] and C_v is the microcanonical heat capacity.[45] For an ensemble of N atoms—i.e., $(3N-6)$ internal degrees of freedom—in a high-temperature harmonic approximation C_v is given by[32,45]

$$C_v = (3N-7)k_B . \quad (4)$$

This definition differs from canonical heat capacity by one unit of k_B. The microcanonical temperature of an isolated cluster describes the average energetic content of an individual degree of freedom, determined by its couplings with the remaining $(3N-7)$ oscillators.[45]

The $(OCS)_n^-$ cluster ions have a variety of modes, not all of which are necessarily equally active in the energy randomization. This can be further complicated by competition with ionic fragmentation. If the electronic-vibrational energy exchange is incomplete on the autodetachment time scale,[33] one could factor in an effective number of degrees of freedom and use it as an adjustable parameter to fit the data. However, we found no need to deviate from the high-temperature microcanonical limit defined by Eq. (4). The microcanonical heat capacity was calculated using this equation with $N=6$, 9, and 12 for $(OCS)_2^-$, $(OCS)_3^-$, and $(OCS)_4^-$, respectively. While the agreement with the experiment does not prove that the decay process is completely statistical, the data do not provide evidence of deviations from the statistical model.

The EAs corresponding to the formation of covalent $(OCS)_2^-$ and its clustered species are not known. As an estimate, we compared the calculated energy of the C_{2v} symmetry dimer anion[3] to the combined energy of two relaxed OCS molecules, as the detachment of $(OCS)_2^-$ can be assumed to be dissociative. The previous study[3] of $(OCS)_2^-$ employed second-order Møller–Plesset perturbation theory with the 6-31+G(d) basis set. However, this method performs poorly in predicting the EA of the OCS monomer. Based on more recent results,[26] we chose a minimal-cost density-functional approach that works well for OCS. In calculations using GAUSSIAN 98,[46] the B3LYP method was used with the 6-31+G(d) and aug-cc-pVDZ basis sets. The results predict the covalent $(OCS)_2^-$ anion to lie 1.01 and 0.98 eV, respectively, lower in energy than two OCS molecules (excluding the zero-point vibrational energy correction). The latter value was adapted as $(OCS)_2^-$ EA in Eq. (3). Accounting for stepwise solvation, the EAs corresponding to $(OCS)_3^-$ and $(OCS)_4^-$ were taken to be 1.25 and 1.5 eV, respectively. The assumed increments correspond to the typical binding energy of OCS in small cluster anions.[47]

The T_{TE} values calculated according to Eqs. (3) and (4) for different cluster sizes and excitation wavelengths are summarized in Table I. These temperatures describe the eKE distributions of the emitted electrons. The high-temperature assumption made in the preceding discussion concerns the significantly higher temperatures of the excited parent clusters, which can be estimated using Eq. (3) without the EA term. Besides, the lowest parent and TE temperatures correspond to the measurements in which only a minor AD component is observed, providing no basis for more careful modeling of the emission process.

TABLE I. TE temperatures (in K) calculated with Eq. (3).

λ (nm)	$(OCS)_2^-$	$(OCS)_3^-$	$(OCS)_4^-$
800	674	246	91
530	1508	704	407
400	2311	1146	712
267	3942	2043	1331

The T_{TE} values from Table I were used with Eq. (2) to model the AD bands in the photoelectron spectra. Their contributions are shown in Figs. 2–4.

Direct photodetachment. The direct photodetachment transitions are characterized in general by anisotropic angular distributions and nonthermal eKE distributions. We model the spectral profile of each of the observed direct detachment bands with

$$P(\varepsilon) = A\varepsilon^{\ell+1/2} \exp[-(h\nu - \varepsilon - \varepsilon_0)^2/w^2], \quad (5)$$

where $(h\nu - \varepsilon)$ is the electron binding energy (eBE). This equation involves two approximations. First, a Gaussian Franck–Condon profile is assumed, with ε_0 corresponding to the VDE and w defining the width. Second, the electronic cross-section scaling is approximated by the pre-Gaussian factor in the form of the Wigner law,[48] assuming an effective free-electron angular momentum quantum number ℓ. This factor is most important for slow electrons, for which the Wigner law is best justified. The coefficient A is proportional (among other factors) to the population of the species responsible for the transition. The variations in A for different transitions as functions of n can be used to gain qualitative insights into the changes in isomer abundances under stepwise solvation.

Except for very slow electrons, ℓ is not as critical in modeling energy spectra as it is for angular distributions.[49,50] Instead of considering the effects of wave interference (nearly impossible in the case of not-well-known electronic structure), we used the dominant ℓ values based on angular anisotropy. In Fig. 1, bands I and II exhibit angular distributions with markedly positive anisotropy parameters,[49,50] characteristic of p_z partial waves (where z is the laser polarization axis). The $\beta>0$ type of transition I is evident in all images, consistent with the detachment from the OCS^- HOMO, previously discussed in the context of photoelectron imaging of $OCS^- \cdot H_2O$.[30] The $\beta>0$ character of band II is best seen in the 400-nm $(OCS)_2^-$ image. Thus we used $\ell=1$ in modeling bands I and II, while the nearly isotropic band III was described by $\ell=0$.

The contributions of bands I, II, and III modeled with Eq. (5) are shown in Figs. 2–4. The sum of all bands, including AD, yields the total simulated spectra shown by bold lines. The only parameter adjusted for AD was its intensity. The low-eKE parts of the spectra, where AD is most impor-

TABLE II. Optimal ε_0 and w values for direct detachment bands in $(OCS)_n^-$ modeled with Eq. (5). Values are listed in eV in the format $\varepsilon_0(w)$. The VDEs are obtained by averaging ε_0 for different wavelengths. Parameters for $OCS^- \cdot H_2O$ (from Ref. 30) are given for comparison.

λ (nm)	$(OCS)_2^-$	$(OCS)_3^-$	$(OCS)_4^-$	$OCS^- \cdot H_2O$
	Band I			
800	1.87 (0.45)	2.15 (0.43)	2.5 (0.48)	2.07 (0.50)
530	1.85 (0.52)	2.15 (0.50)	2.4 (0.48)	2.08 (0.50)
400	1.87 (0.55)	2.20 (0.50)	2.4 (0.48)	2.07 (0.54)
267	1.87 (0.55)	2.10 (0.55)	2.3 (0.55)	
VDE	**1.87**	**2.15**	**2.4**	**2.07**
	Band II			
400	3.40 (0.75)	3.70 (0.75)	3.95 (0.75)	
267	3.40 (0.70)	3.75 (0.70)	3.95 (0.70)	
VDE	**3.40**	**3.73**	**3.95**	
	Band III			
267	3.80 (0.45)	4.15 (0.35)	4.40 (0.40)	
VDE	**3.80**	**4.15**	**4.40**	

tant, are best viewed in the velocity domain. For the direct bands, A, ε_0, and w were adjusted for agreement with the experiment. Discrepancies at the high-eKE tails of the spectra are attributed to the uncorrected backgrounds (proportional to the integration area, increasing for faster electrons and minimally affecting the slow ones) and edge-related artifacts in the images. The contributions of different transitions to the photoelectron images are marked in Fig. 1, while the optimum values of ε_0 and w are summarized in Table II. The VDE values for different transitions in a given cluster, which are also summarized in Table II, were estimated by averaging ε_0 determined at different wavelengths.

V. DISCUSSION

Band assignments. The VDEs associated with the direct detachment bands increase by 0.2–0.3 eV with the addition of each solvent molecule (see Table II). The increase is consistent with the typical binding energy of OCS to a negatively charged cluster core.[3,47]

Band I is consistent with the $OCS^-(OCS)_{n-1}$ structure of the anions responsible for these parts of the images. This can be seen by comparing band I to the $OCS^- \cdot H_2O$ images recorded at the same wavelengths (Fig. 1). In addition, the spectral profiles of band I in Figs. 2(a)–2(c) [$P(\varepsilon)$ columns only] can be compared to the dashed curves representing the fits with Eq. (5) to the $OCS^- \cdot H_2O$ spectra (not shown).[30,31]

The VDE of band I in $(OCS)_2^-$ is 1.87 eV, compared to VDE=2.07 eV for $OCS^- \cdot H_2O$.[30] The mismatch is in line with the difference in solvent binding energies expected for OCS and H_2O [~0.3 eV (Refs. 3 and 47) and 0.5–0.6 eV (Refs. 51 and 52), respectively]. The similarity of the spectra and angular distributions of band I in $(OCS)_2^-$ and $OCS^- \cdot H_2O$ suggests that the structure of the $(OCS)_2^-$ species responsible is likely to be similar to that of $OCS^- \cdot H_2O$. In the latter case, the electrons are ejected from the OCS^- HOMO.[26] Therefore, we attribute band I in $(OCS)_2^-$ to an electrostatically bound isomer described as $OCS^- \cdot OCS$ and the nature of this band is similar to that observed in the photodetachment of $OCS^- \cdot H_2O$.

The significant presence of $OCS^- \cdot OCS$ implies stability of this cluster anion. Given that unsolvated OCS^- is metastable and not formed efficiently in our ion source,[26] the stability of $OCS^- \cdot OCS$ indicates that the EA of OCS is only slightly negative, with its absolute value not exceeding the stabilization energy by one OCS molecule. This observation alone brackets the EA of OCS between approximately −0.3 eV and zero, consistent with the recent indirect estimate of −0.04 eV.[30]

On the other hand, the AD bands indicate the presence of $(OCS)_2^-$, as well as $(OCS)_{3,4}^-$ species with different properties. Since no analog of this signal was seen in $OCS^-(H_2O)_{1,2}$ images,[30] the monomer-based $OCS^-(OCS)_{1-3}$ clusters are unlikely to be responsible for the AD components of the images. Given the lack of anisotropy and considering that the spots appear at $(OCS)_2^-$ image centers at all wavelengths studied, these bands are attributed to an indirect process involving excited anionic states of the covalent dimer, which are not available in $OCS^- \cdot OCS$ or $OCS^- \cdot H_2O$. In the trimer and tetramer, the same excited states of the $(OCS)_2^-$ cluster core are involved. While the involvement of the excited states leaves no doubt, the AD electrons can originate either from these states directly or from the internally excited products of anionic fragmentation that $(OCS)_n^-$ is known to undergo,[3] or from any intermediate configuration.

The existence of the excited states is consistent with the theoretical study of $(OCS)_2^-$, which predicted several low-lying states of the covalent anion of C_{2v} symmetry.[3,29] It is also consistent with the known photochemistry of $(OCS)_n^-$, for which the covalent $(OCS)_2^-$ cluster core is believed to be responsible.[3]

Band II, seen in $(OCS)_n^-$ at 400 and 267 nm, is assigned to direct photodetachment of covalent $(OCS)_2^-$. Just as AD, this band was not seen in $OCS^-(H_2O)_{1-2}$.[30] Its VDE of 3.4 eV is close to the 3.35 eV prediction for the covalent C_{2v} form of $(OCS)_2^-$.[3,29] It is noteworthy that a similar 2.7-eV band in the photoelectron spectrum of $(CS_2)_2^-$ was attributed to a covalent $C_2S_4^-$ anion of C_{2v} symmetry.[19]

Band III observed at 267 nm cannot be assigned unambiguously to any single transition. First, in the energy range where this band is observed we expect several direct detachment transitions from solvated OCS^- accessing the excited states of neutral OCS. For comparison, in 267-nm photodetachment of CS_2^- the transitions to the $a\,^3B_2$, $b\,^3A_2$, and $A\,^1A_2$ neutral states were observed in the range of eBE =3.3–4.1 eV.[19,38] These transitions exhibit either distinctly negative or slightly negative anisotropy,[38] consistent with band III in $(OCS)_{2-4}^-$. Thus, we tentatively assign this band to the analogous neutral states formed in the photodetachment of $OCS^-(OCS)_{1-3}$. In addition, contributions from several singlet and triplet neutral states[29] accessed in the photodetachment of covalent $(OCS)_2^-$ are possible in the same energy range.

Coexistence of isomers. It was previously argued[3] that the relative abundances of the OCS^-- and $(OCS)_2^-$-based clusters may change with cluster size, reminiscent of the core switching[14,18] in $(CO_2)_n^-$ and isomer coexistence[19] in $(CS_2)_n^-$. In this work, the relative intensities of the bands

assigned to $OCS^-(OCS)_{n-1}$ (bands I and III) and $(OCS)_2^-(OCS)_{n-2}$ (AD, band II, and possibly part of band III) shed light on coexistence of the $(OCS)_n^-$ isomers.

The ambiguity in band III assignment leads us to exclude it from this analysis. The AD band also cannot be compared directly to bands I and II, because of the different mechanisms and competition processes involved. Some insight into the changes in isomer abundances with n can be gained by comparing the A factors [Eq. (5)] for bands I and II for clusters of different size. For example, at 400 nm, the I/II ratio, defined as

$$\mathrm{I/II}(n)=\frac{A_{\mathrm{I}}(n)/A_{\mathrm{II}}(n)}{A_{\mathrm{I}}(2)/A_{\mathrm{II}}(2)}, \tag{6}$$

has approximate values of 1, 6, and 4 for $n=2$, 3, and 4, respectively. The implication is that for $(OCS)_3^-$ and $(OCS)_4^-$ the percentage of dimer-based clusters is sixfold and fourfold smaller, respectively, than for $(OCS)_2^-$.

Qualitatively, this trend is seen in Figs. 2(c), 3(c), and 4(c): note the decrease in band II relative contributions for $n=3,4$ compared to $n=2$. Similar conclusions can be drawn from the 267-nm data as well [Figs. 2(d), 3(d), and 4(d)]. However, the above figures obtained with Eq. (6) should be viewed as crude estimates only, because of the approximations inherent in Eq. (5) and the disregard for changes in the electronic cross-sections and Franck–Condon factors upon solvation. Finally, the observed band intensity variations do not correspond exactly to the changes in ''natural'' isomer abundances, as these observations are likely to be affected by the ion source conditions.

Competition of decay mechanisms. Understanding the origin of the autodetached electrons is complicated by the ionic fragmentation processes that excited $(OCS)_n^-$ cluster ions are known to undergo.[3] In principle, the AD electrons can be emitted from (i) the excited parent cluster, (ii) the internally excited anionic fragments, or (iii) an intermediate state of cluster decomposition. We discuss the possible AD pathways in the decay of covalent $(OCS)_2^-$. In larger dimer-based clusters, the same anion is presumed to act as a chromophore and cluster core controlling the decay dynamics.

If the excited $(OCS)_2^-$ decays by autodetachment, the process is bound to be dissociative, most likely yielding two OCS molecules, plus an electron. In ionic fragmentation channels, OCS^-, S_2^- and OCS_2^- products were seen near 800 nm, with the addition of S^- in the vicinity of 400 nm.[3] Of these, metastable OCS^- is a plausible candidate for fragment AD. Given the EAs of OCS, S_2, and S [-0.04 (Ref. 30), 1.67, and 2.1 eV, respectively] and what is known about the $(OCS)_2^-$ dissociation energetics,[3] the adiabatic thresholds for the formation of OCS^-, S_2^-, S^-, and OCS_2^- followed by their AD can be crudely estimated as 0.6, 2.8, 3.7, and 2.8 eV, respectively. Hence, at 800 and 530 nm, only the OCS^- fragment AD is possible. At 400 nm, two additional pathways may be accessible, but given no significant increase in the AD signal, we restrict the discussion to OCS^- as the most plausible source of fragment AD. At 267 nm, all of the above ionic fragments can be formed above their respective detachment thresholds, which may account for the sharp increase in AD at 267 nm compared to other wavelengths.

Considering the 800–400 nm excitations, two AD pathways are most likely for $(OCS)_2^-$:

$$[(OCS)_2^-]^* \xrightarrow{\mathrm{AD}} (OCS)_2 + e^- \rightarrow OCS + OCS + e^-, \tag{7a}$$

$$[(OCS)_2^-]^* \rightarrow OCS + OCS^- \xrightarrow{\mathrm{AD}} OCS + OCS + e^-, \tag{7b}$$

where $*$ denotes the excited parent state. The TE model of autodetachment employed in Sec. IV does not distinguish between these pathways. It assumes only that the energy is divided randomly among all product degrees of freedom. Since the final products are the same, Eqs. (7a) and (7b) describe different pathways of the same decomposition reaction. In a statistical regime, one cannot specify at what stage of complex disintegration the electron leaves the nuclear framework. However, if the ionic fragmentation were fast, pathway (7b) could possibly dominate. In this case, the impulsive dissociation would be expected to result in nonstatistical energy partitioning.

Although there is not enough information to conclusively discriminate between pathways (7a) and (7b), or in fact to provide a rigorous proof of the statistical nature of the decay process, the performance of the TE model gives no justification for invoking nonstatistical dynamics. The multiple fragmentation channels active in the decay also point away from impulsive dissociation. Finally, recent experiments on $(CS_2)_2^-$ by Mabbs *et al.*[22] revealed no significant reduction in AD at 400 and 530 nm, compared to $(OCS)_2^-$. This observation is inconsistent with the AD originating primarily from the fragments, because CS_2^-, the most likely source of fragment AD in the $(CS_2)_2^-$ case, is 0.9 eV more stable to detachment than OCS^-.

We now consider the sharp drop in relative AD intensity from $(OCS)_2^-$ to $(OCS)_3^-$, followed by a less significant decrease in $(OCS)_4^-$. While the drop is particularly drastic at 400 nm and longer wavelengths, it is also significant at 267 nm. There are two possible reasons for this effect: (i) the decrease in the relative abundance of $(OCS)_2^-(OCS)_{n-2}$ and (ii) the competition of electron emission with cluster fragmentation.

First, there is a decrease in the relative abundance of $(OCS)_2^-(OCS)_{n-2}$ ions for $n=3$ and 4, compared to $n=2$. This is revealed in the images (Fig. 1) and spectra (Figs. 2–4) by the weakening intensity of band II relative to band I. However, comparing Figs. 2(c) and 3(c), we note that the decrease in AD from $(OCS)_2^-$ to $(OCS)_{3,4}^-$ is more significant than the corresponding drop in band II intensity. If the same cluster type (dimer based) is responsible for both AD and band II, the isomer abundance argument is not sufficient to describe the observed trend. The greater number of degrees of freedom in larger clusters, resulting in lower TE temperatures and longer emission lifetimes, can contribute to lowering the AD intensity, but only if the electron emission competes with another excited-state decay mechanism.

The drop in AD intensity should be considered in the context of changes occurring in the ionic fragmentation channels. In $(OCS)_n^-$ dissociation, the fractional yield of

S_2^- nearly doubles for $(OCS)_3^-$ compared to $(OCS)_2^-$ at both 790 and 395 nm, while the 395 nm yield of OCS^- drops from 8% to zero.[3] These changes in the fragmentation channels show that solvation affects the excited cluster decay mechanism.

In covalent $(OCS)_2^-$, dissociation involves the breaking of covalent bonds. The energy barriers involved, which could be comparable to the electron emission barrier, indirectly contribute to making the competing process, the autodetachment, more favorable. In $(OCS)_{3,4}^-$, solvation increases the electron detachment energy, while enabling cluster relaxation by solvent evaporation. Fragmentation can thus become a preferred decay mechanism.

For all cluster sizes studied, the relative AD intensity increases sharply at 267 nm compared to longer wavelengths. This could be a consequence of two effects: (i) a decrease in the parent AD lifetime, favoring electron emission over ionic fragmentation, and (ii) an increase in fragment–ion internal excitation, leading to a corresponding increase in fragment AD. The congestion of low-eKE bands at 267 nm does not allow for a careful analysis of the separate transitions. In particular, our confidence in the assigned TE temperatures (Table I) and even the applicability of the statistical description at 267 nm is not as high as at lower photon energies.

Applicability of statistics. Finally, we comment on the performance of the statistical TE model in describing the autodetachment of the rather small gas-phase systems studied in this work. The agreement between the model and the slow-electron parts of the experimental spectra is best examined in the $P(v)$ columns of Figs. 2–4.

Although the quantitative agreement is quite remarkable, it can be potentially misleading. Caution is necessary in interpreting its significance, because the AD bands overlap with direct detachment transitions. In addition, in some cases the AD intensities are so low that the data allow, in fact, for only a qualitative interpretation. Thus, for $(OCS)_{3,4}^-$ at 800, 530, and 400 nm, the data indicate the presence of isotropic slow-electron components attributed to AD. While these weak contributions are described adequately by the statistical model, the agreement is not a rigorous proof of the statistical nature of the decay.

Another word of caution applies to some of the low TE temperatures predicted by the model, such as $T_{TE}=91$ K for $(OCS)_4^-$ at 800 nm (see Table I). Although the corresponding microcanonical temperature of the excited cluster prior to electron emission is much higher (691 K in the above example), one may still question the validity of the high-temperature harmonic assumption inherent in the model. In addition, in the low-temperature regime, T_{TE} is extremely sensitive to the value of EA in Eq. (3). Since the electron affinities used are approximate, only limited confidence can be placed in the lowest T_{TE} values in Table I. However, this uncertainty does not affect modeling of the data: the simulated spectrum in Fig. 4(a) agree well with the experiment, because the AD is so weak that T_{TE} could be varied over a wide range without affecting significantly the quality of the agreement.

Overall, we conclude that the observed spectral signatures of autodetachment are consistent with the statistical model. In those cases, when the AD component is strong—e.g., $(OCS)_2^-$—there is sufficient confidence in the agreement between the experiment and theory to argue that the assumptions of strong electronic–vibrational couplings and energy redistribution are indeed applicable to the covalent dimer ion. However, even for $(OCS)_2^-$, there is not enough basis for arguing the finer details of the model, such as the exact extent of participation of different degrees of freedom and distinguishing between the excited parent and fragment autodetachment.

VI. SUMMARY

This study is an attempt to decipher the structure of $(OCS)_n^-$ cluster anions using photoelectron spectroscopy. The employed imaging approach is key to assignment of the observed transitions, as it allows the simultaneous examination of energy spectra and angular distributions of both fast and slow photoelectrons.

The results provide spectroscopic evidence of the coexistence of electronic and structural isomers of $(OCS)_n^-$ with the OCS^- and covalently bound $(OCS)_2^-$ cluster cores. The $OCS^-(OCS)_{n-1}$ and $(OCS)_2^-(OCS)_{n-2}$ anions respond differently to photoexcitation. The OCS^--based clusters exhibit direct photodetachment. The dimer-based clusters can be either photodetached directly or promoted to an excited anionic state. The subsequent decay, in turn, involves the competition between autodetachment and fragmentation.

The autodetachment can originate from either the excited parent clusters or internally excited anionic fragments (or an intermediate state). Regardless of the pathway, the electron spectra are described successfully using a thermionic-emission model, which assumes strong electronic–vibrational couplings and statistical energy partitioning among product degrees of freedom. The AD cross section in the trimer and the tetramer anions decreases relative to the dimer anion. It is suggested that this effect reflects the competition between the AD and fragmentation channels.

ACKNOWLEDGMENTS

The authors thank Dr. R. Mabbs for discussions of this work and comments on the manuscript. We also thank V. Dribinski and Professor H. Reisler for providing the image analysis software. Discussions with Professor W. C. Lineberger and Professor K. D. Jordan are gratefully acknowledged. This work is supported by NSF Grants No. CHE-9982057 and No. CHE-0134631, a Beckman Young Investigator Award, ACS PRF Grant No. 35589-G6, and Research Corporation Research Innovation Award No. RI0515. A.S. is a David and Lucile Packard Foundation Fellow.

[1] A. W. Castleman and K. H. Bowen, J. Phys. Chem. **100**, 12911 (1996).
[2] J. Jortner, U. Even, A. Goldberg, I. Schek, T. Raz, and R. D. Levine, Surf. Rev. Lett. **3**, 263 (1996).
[3] A. Sanov, S. Nandi, K. D. Jordan, and W. C. Lineberger, J. Chem. Phys. **109**, 1264 (1998).
[4] C. E. Klots and R. N. Compton, J. Chem. Phys. **67**, 1779 (1977).
[5] C. E. Klots and R. N. Compton, J. Chem. Phys. **69**, 1636 (1978).
[6] M. Knapp, D. Kreisle, O. Echt, K. Sattler, and E. Recknagel, Surf. Sci. **156**, 313 (1985).

[7] M. Knapp, O. Echt, D. Kreisle, T. D. Mark, and E. Recknagel, Chem. Phys. Lett. **126**, 225 (1986).
[8] A. Stamatovic, K. Leiter, W. Ritter, K. Stephan, and T. D. Mark, J. Chem. Phys. **83**, 2942 (1985).
[9] H. Langosh and H. Haberland, Z. Phys. D: At., Mol. Clusters **2**, 243 (1986).
[10] T. Kondow and K. Mitsuke, J. Chem. Phys. **83**, 2612 (1985).
[11] T. Kondow, J. Phys. Chem. **91**, 1307 (1987).
[12] M. L. Alexander, M. A. Johnson, N. E. Levinger, and W. C. Lineberger, Phys. Rev. Lett. **57**, 976 (1986).
[13] K. H. Bowen and J. G. Eaton, in *The Structure of Small Molecules and Ions*, edited by R. Naaman and Z. Vager (Plenum, New York, 1988), p. 147.
[14] M. J. DeLuca, B. Niu, and M. A. Johnson, J. Chem. Phys. **88**, 5857 (1988).
[15] T. Kraft, M. W. Ruf, and H. Hotop, Z. Phys. D: At. Mol. Clusters **14**, 179 (1989).
[16] F. Misaizu, K. Mitsuke, T. Kondow, and K. Kuchitsu, J. Chem. Phys. **94**, 243 (1991).
[17] K. Hiraoka, S. Fujimaki, G. Aruga, and S. Yamabe, J. Phys. Chem. **98**, 1802 (1994).
[18] T. Tsukuda, M. A. Johnson, and T. Nagata, Chem. Phys. Lett. **268**, 429 (1997).
[19] T. Tsukuda, T. Hirose, and T. Nagata, Chem. Phys. Lett. **279**, 179 (1997).
[20] T. Maeyama, T. Oikawa, T. Tsumura, and N. Mikami, J. Chem. Phys. **108**, 1368 (1998).
[21] H. Chen, R. B. Huang, X. Lu, Z. C. Tang, X. Xu, and L. S. Zheng, J. Chem. Phys. **112**, 9310 (2000).
[22] R. Mabbs, E. Surber, and A. Sanov (unpublished).
[23] S. H. Fleischman and K. D. Jordan, J. Phys. Chem. **91**, 1300 (1987).
[24] A. Sanov, W. C. Lineberger, and K. D. Jordan, J. Phys. Chem. A **102**, 2509 (1998).
[25] S. Koizumi, H. Yasumatsu, S. Otani, and T. Kondow, J. Phys. Chem. A **106**, 267 (2002).
[26] E. Surber, S. P. Ananthavel, and A. Sanov, J. Chem. Phys. **116**, 1920 (2002).
[27] G. L. Gutsev, R. J. Bartlett, and R. N. Compton, J. Chem. Phys. **108**, 6756 (1998).
[28] M. A. Johnson (personal communication).
[29] A. Sanov, W. C. Lineberger, and K. D. Jordan (unpublished).
[30] E. Surber and A. Sanov, J. Chem. Phys. **116**, 5921 (2002).
[31] E. Surber and A. Sanov, Phys. Rev. Lett. **90**, 093001 (2003).
[32] B. Baguenard, J. C. Pinare, C. Bordas, and M. Broyer, Phys. Rev. A **63**, 023204 (2001).
[33] J. U. Andersen, E. Bonderup, and K. Hansen, J. Phys. B **35**, R1 (2002).
[34] P. Wurz and K. R. Lykke, J. Phys. Chem. **96**, 10129 (1992).
[35] Y. X. Zhao, E. Debeer, C. S. Xu, T. Taylor, and D. M. Neumark, J. Chem. Phys. **105**, 4905 (1996).
[36] B. Baguenard, J. C. Pinare, F. Lepine, C. Bordas, and M. Broyer, Chem. Phys. Lett. **352**, 147 (2002).
[37] D. W. Chandler and P. L. Houston, J. Chem. Phys. **87**, 1445 (1987).
[38] E. Surber, R. Mabbs, and A. Sanov (unpublished).
[39] M. A. Johnson and W. C. Lineberger, in *Techniques for the Study of Ion Molecule Reactions*, edited by J. M. Farrar and J. W. Saunders (Wiley, New York, 1988), p. 591.
[40] L. A. Posey, M. J. Deluca, and M. A. Johnson, Chem. Phys. Lett. **131**, 170 (1986).
[41] A. T. J. B. Eppink and D. H. Parker, Rev. Sci. Instrum. **68**, 3477 (1997).
[42] A. J. R. Heck and D. W. Chandler, Annu. Rev. Phys. Chem. **46**, 335 (1995).
[43] V. Dribinski, A. Ossadtchi, V. A. Mandelshtam, and H. Reisler, Rev. Sci. Instrum. **73**, 2634 (2002).
[44] C. E. Klots, J. Chem. Phys. **100**, 1035 (1994).
[45] J. U. Andersen, E. Bonderup, and K. Hansen, J. Chem. Phys. **114**, 6518 (2001).
[46] M. J. Frisch *et al.*, computer code GAUSSIAN 98, Rev. A.7, Gaussian, Inc., 1998.
[47] S. Nandi, A. Sanov, N. Delaney, J. Faeder, R. Parson, and W. C. Lineberger, J. Phys. Chem. A **102**, 8827 (1998).
[48] E. P. Wigner, Phys. Rev. **73**, 1002 (1948).
[49] J. Cooper and R. N. Zare, J. Chem. Phys. **48**, 942 (1968).
[50] J. Cooper and R. N. Zare, in *Atomic Collision Processes*, edited by S. Geltman, K. T. Mahanthappa, and W. E. Brittin (Gordon and Breach, New York, 1968), Vol. XI-C, p. 317.
[51] A. W. Castleman and R. G. Keesee, Annu. Rev. Phys. Chem. **37**, 525 (1986).
[52] T. Tsukuda, M. Saeki, R. Kimura, and T. Nagata, J. Chem. Phys. **110**, 7846 (1999).